^{18}F-Fluorosulfate for PET Imaging of the Sodium–Iodide Symporter: Synthesis and Biologic Evaluation In Vitro and In Vivo

Alex Khoshnevisan[1], Krisanat Chuamsaamarkkee[1], Mehdi Boudjemeline[1], Alex Jackson[2], Gareth E. Smith[2], Antony D. Gee[1], Gilbert O. Fruhwirth[1], and Philip J. Blower[1]

[1]Division of Imaging Sciences and Biomedical Engineering, St. Thomas' Hospital, King's College London, London, United Kingdom; and [2]GE Healthcare, Amersham, United Kingdom

Anion transport by the human sodium–iodide symporter (hNIS) is an established target for molecular imaging and radionuclide therapy. Current radiotracers for PET of hNIS expression are limited to $^{124}I^-$ and $^{18}F\text{-}BF_4^-$. We sought new ^{18}F-labeled hNIS substrates offering higher specific activity, higher affinity, and simpler radiochemical synthesis than $^{18}F\text{-}BF_4^-$. **Methods:** The ability of a range of anions, some containing fluorine, to block $^{99m}TcO_4^-$ uptake in hNIS-expressing cells was measured. SO_3F^- emerged as a promising candidate. $^{18}F\text{-}SO_3F^-$ was synthesized by reaction of $^{18}F^-$ with SO_3–pyridine complex in MeCN and purified using alumina and quaternary methyl ammonium solid-phase extraction cartridges. Chemical and radiochemical purity and serum stability were determined by radiochromatography. Radiotracer uptake and efflux in hNIS-transduced HCT116-C19 cells and the hNIS-negative parent cell line were evaluated in vitro in the presence and absence of a known competitive inhibitor ($NaClO_4$). PET/CT imaging and ex vivo biodistribution measurement were conducted on BALB/c mice, with and without $NaClO_4$ inhibition. **Results:** Fluorosulfate was identified as a potent inhibitor of $^{99m}TcO_4^-$ uptake via hNIS in vitro (half-maximal inhibitory concentration, 0.55–0.56 μM (in comparison with 0.29–4.5 μM for BF_4^-, 0.07 μM for TcO_4^-, and 2.7–4.7 μM for I^-). Radiolabeling to produce $^{18}F\text{-}SO_3F^-$ was simple and afforded high radiochemical purity suitable for biologic evaluation (radiochemical purity > 95%, decay-corrected radiochemical yield = 31.6%, specific activity ≥ 48.5 GBq/μmol). Specific, blockable hNIS-mediated uptake in HCT116-C19 cells was observed in vitro, and PET/CT imaging of normal mice showed uptake in thyroid, salivary glands (percentage injected dose/g at 30 min, 563 ± 140 and 32 ± 9, respectively), and stomach (percentage injected dose/g at 90 min, 68 ± 21). **Conclusion:** Fluorosulfate is a high-affinity hNIS substrate. $^{18}F\text{-}SO_3F^-$ is easily synthesized in high yield and very high specific activity and is a promising candidate for preclinical and clinical PET imaging of hNIS expression and thyroid-related disease; it is the first example of in vivo PET imaging with a tracer containing an S–^{18}F bond.

Key Words: human sodium/iodide symporter (SC5A5); fluorosulfate; ^{18}F; PET; thyroid

J Nucl Med 2017; 58:156–161
DOI: 10.2967/jnumed.116.177519

The sodium–iodide symporter (NIS) is capable of intracellularly concentrating certain small anions against their electrochemical gradient and is biologically important for accumulating iodide in thyroid follicles for synthesis of thyroid hormones. Several radioactive substrates of human NIS (hNIS; SC5A5) have been used for radionuclide therapy ($^{131}I^-$) and SPECT ($^{131/123}I^-$, $^{99m}TcO_4^-$) and PET ($^{124}I^-$) imaging of thyroid-related disorders (*1*). Other radioactive substrates currently being evaluated as next-generation radiopharmaceuticals for these purposes include $^{186/188}ReO_4^-$ for therapy (*2,3*) and $^{18}F\text{-}BF_4^-$ for PET (*4,5*). $^{18}F\text{-}BF_4^-$ is the prototype ^{18}F-labeled NIS tracer, offering the advantages of moderate half-life, excellent imaging characteristics associated with a high yield of low-energy positrons, minimal undesirable photon emissions, low absorbed radiation dose (*6*), and wide availability. With these characteristics, it is expected to offer imaging superior to that of SPECT with $^{123/131}$I and PET with ^{124}I. However, among the known substrates of NIS, it has mid-ranking affinity (half-maximal inhibitory concentration [IC_{50}] of 1.2 μM for inhibition of $^{124}I^-$ uptake, in comparison with an IC_{50} of 0.1 μM for ClO_4^- in the same assay (*7*)), and chemical constraints during synthesis lead to low specific activity (*4,8*). Consequently, alternative ^{18}F-labeled NIS substrates that overcome these limitations are desirable.

A search of the literature for alternative fluorine-containing NIS substrates reveals several that merit further investigation. Both SO_3F^- and $PO_2F_2^-$ are known to inhibit radioiodide uptake in mouse thyroid (*9*), yet in quantitative terms their effectiveness as substrates or inhibitors of hNIS is unknown. PF_6^- is a highly potent inhibitor of rat NIS (IC_{50}, 15 nM (*10*)). We therefore performed a preliminary comparison of their ability to inhibit hNIS, using uptake in hNIS-expressing cells with ^{99m}Tc-pertechnetate as a probe. From this survey we selected SO_3F^- on the basis of its high affinity and potentially straightforward radiolabeling.

Here we report a comparison of fluorine-containing anions with other known hNIS substrates and, for the first time, a simple method for radiosynthesis of $^{18}F\text{-}SO_3F^-$ and its biologic evaluation in hNIS-expressing cells and in vivo in mice.

MATERIALS AND METHODS

General

Unless otherwise stated, all chemicals were from Sigma Aldrich. Ammonium difluorophosphate was synthesized as previously described (*11*) (the nuclear magnetic resonance data are in Supplemental Figs. 1 and

Received May 16, 2016; revision accepted Jul. 11, 2016.
For correspondence or reprints contact: Philip J. Blower, King's College London, Division of Imaging Sciences and Biomedical Engineering, 4th Floor, Lambeth Wing, St. Thomas' Hospital, London SE1 7EH, United Kingdom.
E-mail: philip.blower@kcl.ac.uk.
Published online Aug. 18, 2016.

2; supplemental materials are available at http://jnm.snmjournals.org). $^{18}F^-$ was produced as previously described (*4*). $^{99m}TcO_4^-$ was obtained from Guy's Hospital Radiopharmacy and was used about 4.5 h after elution (24 h between elutions). Animal experiments were performed under a U.K. Home Office license following the guidance of the U.K. Research Councils and the Medical Research Charities on responsibility in the use of animals in bioscience research, as approved by the local institutional ethics committee. Inhibitory potency was assessed by pertechnetate uptake blockade, using 2 different cell lines expressing hNIS: a virally infected breast adenocarcinoma cell line stably expressing hNIS (MTLn3E.Δ34 CXCR4-eGFP hNIS-tag-RFP, hereinafter referred to as 3E.Δ-NIS (*12*)) and a human colon carcinoma cell line transfected to stably express hNIS under selection pressure (HCT116-hNIS-C19 (*5*)). Parental cell lines served as negative controls. HCT116 was also used to study the cellular uptake of $^{18}F\text{-}SO_3F^-$ in the absence of hNIS. Ionic volumes were either taken directly from the literature (*13*) or calculated from crystallographic data using previously described methods ($PO_2F_2^-$ (*14*); TcO_4^- (*15,16*)).

Optimized Radiosynthesis

The following procedure was arrived at after optimization of reaction time, temperature, and conditions. Solutions of K_2CO_3 (5.2 mg) in H_2O (0.4 mL) and of K[2.2.2] (14.2 mg) in MeCN (1.1 mL) were prepared. K_2CO_3 solution (0.2 mL) was added to the K[2.2.2] solution to form quaternary methyl ammonium eluent. ^{18}F-fluoride was trapped from $^{18}O\text{-}H_2O$ on a quaternary methyl ammonium cartridge (preconditioned with $NaHCO_3$ [10 mL] and H_2O [10 mL]), eluted with quaternary methyl ammonium eluent (0.9 mL), and dried by azeotropic distillation of MeCN (0.4 mL) under a N_2 stream at 110°C for 5 min and then twice further at 95°C. SO_3–pyridine complex (5 mg) in MeCN (1 mL) was then added, followed by heating to 80°C for 10 min. The reaction was quenched with H_2O (2 mL), and the solution was passed through a neutral alumina cartridge (preconditioned with H_2O [20 mL] and air [10 mL]) and a quaternary methyl ammonium cartridge (preconditioned with 1 M NaCl [5 mL] and H_2O [10 mL]). The quaternary methyl ammonium was washed with H_2O (4 mL), and the product was eluted with 0.9% NaCl (0.4 mL), ready for biologic evaluation. Radio–thin-layer chromatography (R_f values, 0.43 for SO_3F^- and 0 for F^-) was performed using a neutral alumina stationary phase (10 × 80 mm, Polygram ALOX N/UV_{254}; Machery-Nagel) and a methanol mobile phase on a Mini-Scan scanner (LabLogic) with a β^+ probe (B-FC-3600; LabLogic). Radiochemical identity, purity, specific activity, and sulfate concentration were established by ion chromatography (930 Compact IC Flex; Metrohm) with in-line conductimetric and γ-detectors, using a I-524A ion chromatography column (4.6 × 100 mm; Shodex) eluted with aqueous 2.3 mM phthalic acid and 2.3 mM tris(hydroxymethyl)aminomethane (pH 5.0) at a flow rate of 1.5 mL/min and a column temperature of 30°C. The limit of detection was 894 ng/mL for KSO_3F. Pyridine was determined by high-performance liquid chromatography (1200 series; Agilent), with the ultraviolet/visible detector adjusted to 210 nm, on a Zorbax 300-SCX column (Agilent) eluted with 0.2 M sodium phosphate, pH 3, at 1.0 mL/min. The K[2.2.2] concentration was determined as described previously (*17*).

$^{99m}TcO_4^-$ Uptake Inhibition Assay (HCT116-hNIS-C19 Cells)

HCT116-hNIS-C19 cells seeded in 12-well plates (5×10^5 cells per well) were incubated with 5% CO_2 at 37°C for 24 h, washed twice with Hanks balanced salt solution (HBSS), and then incubated for 30 min in HBSS with the chosen inhibitory anion (700 μL of a 1×10^{-2} to 1×10^{-13} M concentration, $n = 3$ each). $^{99m}TcO_4^-$ (0.1 MBq, ~37 pM) in HBSS (50 μL) was added, followed by 30 min of incubation. The medium was removed, and the cells were washed with HBSS (750 μL) and extracted with 1 M NaOH (750 μL). Bound radioactivity and unbound radioactivity were γ-counted. IC_{50} values were determined by least-squares fitting of a sigmoidal curve (Prism, version 5.03; GraphPad).

$^{99m}TcO_4^-$ Uptake Inhibition Assay (3E.Δ-NIS Cells)

3E.Δ-NIS cells seeded in 6-well plates were incubated as above for 12 h, washed with phosphate-buffered saline (1 mL), incubated with phosphate-buffered saline (1 mL) containing the inhibitor (range, 1×10^{-11} to 5×10^{-4} M, $n = 3$ each) and $^{99m}TcO_4^-$ (50 kBq/mL, ~14 pM) for 30 min, washed twice with phosphate-buffered saline (1.4 mL), trypsinized (900 μL of 250 U.S. Pharmacopeia trypsin units/mg in phosphate-buffered saline) at 37°C for 5 min, resuspended in phosphate-buffered saline (250 μL), and centrifuged. Cell-bound and combined media and washings were γ-counted. Data were fitted to sigmoidal curves using Origin, version 8.0 (Microcal).

Stability Studies

$^{18}F\text{-}SO_3F^-$ was incubated in 0.9% NaCl or 50 mM glycine/HCl buffer (pH 3.0) at 25°C for 4 h and analyzed by ion chromatography and thin-layer chromatography as described above. $^{18}F\text{-}SO_3F^-$ (~25 MBq) in 0.9% NaCl (100 μL) was incubated with human serum (1 mL) at 37°C for 4 h. Hourly samples (100 μL) were mixed with ethanol (100 μL) to precipitate proteins and were centrifuged, and the supernatants were analyzed by thin-layer chromatography.

$^{18}F\text{-}SO_3F^-$ Cell-Binding Study

HCT116-hNIS-C19 or HCT116 cells seeded in 6-well plates (1×10^6 cells per well) were incubated as above for 24 h, washed twice with HBSS, and incubated in HBSS (950 μL) with or without $NaClO_4$ (20 μM) for 30 min. $^{18}F\text{-}SO_3F^-$ (0.1 MBq) in HBSS (50 μL) was then added, followed by incubation for 30 min (in triplicate). The cells were washed with HBSS (1 mL) and extracted with 1 M NaOH (1 mL), and the cell extract and medium/washings were γ-counted. Intracellular-to-extracellular concentration ratios were estimated using a mean cell diameter of 18.4 μm (*18*).

$^{18}F\text{-}SO_3F^-$ Self-Inhibition

HCT116-hNIS-C19 cells seeded in 12-well plates (5×10^5/well) were incubated as above for 24 h, washed twice with HBSS, and incubated with KSO_3F (range, 1×10^{-2} to 10^{-12} M, $n = 3$ each) in HBSS (700 μL) for 30 min. $^{18}F\text{-}SO_3F^-$ (0.1 MBq) in HBSS (50 μL) was then added and incubated for 30 min. The cells were washed and counted, and IC_{50} was determined as above.

$^{18}F\text{-}SO_3F^-$ Cell Efflux

HCT116-hNIS-C19 cells were prepared as for the self-inhibition experiment above, incubated with $^{18}F\text{-}SO_3F^-$ (0.1 MBq) in HBSS (750 μL) for 60 min, and washed with cold HBSS (750 μL) before the addition of fresh tracer-free medium. The cells and medium were sampled and γ-counted as described above.

PET Imaging

Female BALB/c mice (4–8 wk old) were given either $NaClO_4$ (250 mg/kg intraperitoneal injection as a competitive substrate for inhibitive effect) in 0.9% NaCl or an equal volume of plain 0.9% NaCl (sham inhibitor). One hour later, $^{18}F\text{-}SO_3F^-$ (~5 MBq in 0.9% NaCl, 150 μL) was injected (tail vein) under anesthesia maintained using 1.5%–2% isoflurane gas (Isocare; Animalcare) in O_2. The mice were then transferred to the warmed scanner bed while anesthesia was maintained and vital signs monitored. Dynamic PET was acquired for 2 h (starting <1 min after tracer injection) on the nanoScan PET/CT scanner (Mediso) in list mode using a 400- to 600-keV energy window and a coincidence relation of 1:3, followed by CT (55-keV x-rays, 1,000-ms exposure, 360 projections, and 1 pitch). The PET data were processed with Tera-tomo software (supplied with the system), applying corrections for attenuation, scatter, and dead time; rebinned;

and reconstructed into a series of 5-min frames for the first 30 min and 30-min frames thereafter. VivoQuant (InviCro) software was used to view and quantify the data. Regions of interest were manually drawn over thyroid, salivary glands, stomach, bladder, left ventricle (for blood), and muscle at a threshold of 10% of the maximum count to define the edges. Time–activity curves were generated and expressed as percentage injected dose (%ID, with whole-body region-of-interest activity, excluding tail, as the injected dose) and %ID per ex vivo weight of organ (%ID/g).

Ex Vivo Biodistribution

At 2.25 h after injection, the scanned mice were sacrificed by cervical dislocation and the tissues were harvested, weighed, and γ-counted (channels 175–220, 1282 Compugamma; LKB). Data are presented as %ID/g (with total activity of all body parts—including carcass and any urine excreted at the time of sacrifice but excluding the tail—as the injected dose). Calculations requiring thyroid weight were conducted using a standard weight of 3.6 mg (*4,19*).

RESULTS

$^{99m}TcO_4^-$ Uptake Inhibition Assay

The IC_{50} for the anions assessed for their ability to block $^{99m}TcO_4^-$ or $^{18}F\text{-}BF_4^-$ uptake via hNIS are detailed in Supplemental Table 1, which also includes comparable literature data (*5,7,8,10,20*)). The potency was in the order $SCN^- < PO_2F_2^- < I^- < BF_4^- \approx SO_3F^- < ReO_4^- < TcO_4^- < PF_6^-$, which roughly parallels the increase in ionic volume (Fig. 1). Literature data on inhibitory potency and affinity of anions are not comprehensive but when available are broadly consistent with our results. Of the fluorine-containing substrates, PF_6^- (IC_{50}, 21 nM) was the most potent, but SO_3F^- had potency (IC_{50}, 0.56 μM) comparable to BF_4^- and better than iodide (IC_{50}, >2.7 mM) and is more likely to be amenable to simple radiosynthesis than BF_4^- or PF_6^-. SO_3F^- was therefore selected for development of a new PET tracer.

Radiosynthesis of $^{18}F\text{-}SO_3F^-$

Reaction of K[2.2.2]/^{18}F-KF with SO_3–pyridine complex (Fig. 2) afforded $^{18}F\text{-}SO_3F^-$. Varying the reaction conditions (Supplemental Table 2) led to crude radiochemical yields of as high as 65%. Passage through an alumina column removed unreacted $^{18}F^-$, and the eluted product could be trapped on a quaternary methyl ammonium cartridge, allowing washing to remove pyridine and K[2.2.2], and eluted in 0.9% NaCl (radiochemical yield, 31.6% ± 9.5% [n = 3, decay corrected]; radiochemical purity, 96% ± 1% [always ≥ 95%]). The total synthesis time from end of bombardment was less than 1 h. The identity of the product was confirmed by ion chromatography with coinjection of authentic SO_3F^- as a reference (Fig. 3). With a starting radioactivity of about 750 MBq, a specific activity of at least 48.5 ± 13.4 GBq/μmol (n = 3) was obtained in a volume of 0.4 mL. The product contained residual pyridine (1.4 ± 1 μg/mL, 0.56 μg total), K[2.2.2] (<6.25 μg/mL, <2.5 μg total), and SO_4^{2-} (302 ± 26 μg/mL, 120.7 μg total) and had a pH of 7.

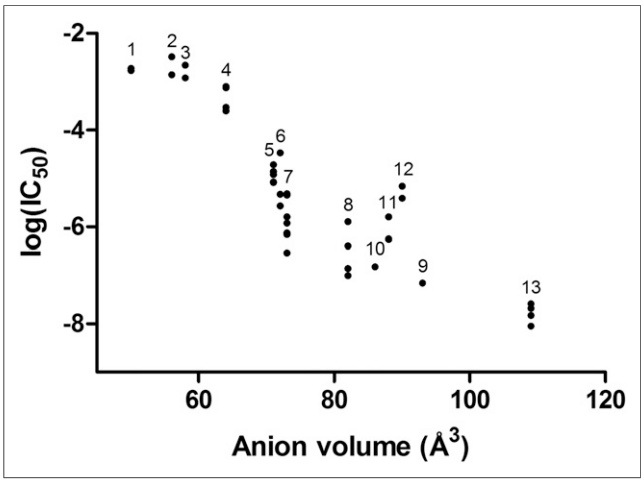

FIGURE 1. Plot of ionic volume against inhibitory potency ($\log IC_{50}$ based on ability to block anion uptake in NIS-expressing cells) for univalent anions examined in this work and other published works (*5–7,9,17*). Differing methods, cell lines, probes, and counter-ions were used in each study; further details are given in Supplemental Table 1. 1 = CN^-; 2 = Br^-; 3 = N_3^-; 4 = NO_3^-; 5 = SCN^-; 6 = I^-; 7 = BF_4^-; 8 = ClO_4^-; 9 = TcO_4^-; 10 = ReO_4^-; 11 = SO_3F^-; 12 = $PO_2F_2^-$; 13 = PF_6^-.

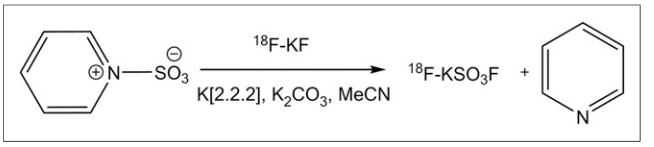

FIGURE 2. Reaction scheme for production of $^{18}F\text{-}SO_3F^-$ from SO_3–pyridine complex.

In Vitro Uptake, Efflux, and Self-Inhibition of $^{18}F\text{-}SO_3F^-$

Significant uptake of the radiotracer in hNIS-expressing HCT116-C19 cells was observed and was blocked by $NaClO_4$ (Fig. 4). No uptake occurred in the parental cell line HCT116 (which does not express hNIS), with or without $NaClO_4$. Both uptake and efflux from the cells reached equilibrium within 80 min (Supplemental Figs. 3 and 4). Uptake at equilibrium was consistent with an intracellular-to-extracellular $^{18}F\text{-}SO_3F^-$ concentration ratio of 76:1. Under identical conditions, the ratio for $^{99m}TcO_4^-$ was 44:1 and that for $^{18}F\text{-}BF_4^-$ was 24:1 (calculated from data obtained during this and other studies (*7*), respectively). Inhibition of $^{18}F\text{-}SO_3F^-$ uptake in HCT116-C19 cells by KSO_3F occurred with an IC_{50} of 1.6 μM (Fig. 5).

Serum Stability

Ion chromatography and thin-layer chromatography of the tracer both as formulated and under acidic conditions (pH 3.0) were unchanged (radiochemical purity > 95%) after 4 h at room temperature. Similarly, the radiochemical purity was more than 95% after 4 h of incubation (37°C) in serum, as assessed by thin-layer chromatography of the supernatant after protein precipitation with ethanol (no significant radioactivity was associated with the protein pellet). These data are summarized in Supplemental Table 3.

PET/CT Imaging

PET/CT of $^{18}F\text{-}SO_3F^-$ (Fig. 6) revealed prominent uptake in the thyroid, stomach, and salivary glands of normal mice, but this uptake was suppressed in the perchlorate-treated mice. Time–activity curves (%ID/g, Supplemental Figs. 5 and 6; %ID, Supplemental Figs. 7 and 8) over a 2-h imaging period showed thyroid and salivary gland uptake plateauing at around 30–45 min (563 ± 140 and 32 ± 9 %ID/g, respectively, at 30 min) and stomach uptake plateauing at around 90 min (68 ± 21 %ID/g at 90 min). Bone uptake first became detectable at 30 min and increased to 3 ± 1 %ID/g by 60 min.

Ex Vivo Biodistribution in Mice

At 2.25 h after injection, uptake of $^{18}F\text{-}SO_3F^-$ consistent with the PET scans was observed in thyroid (144 ± 71 %ID/g), stomach

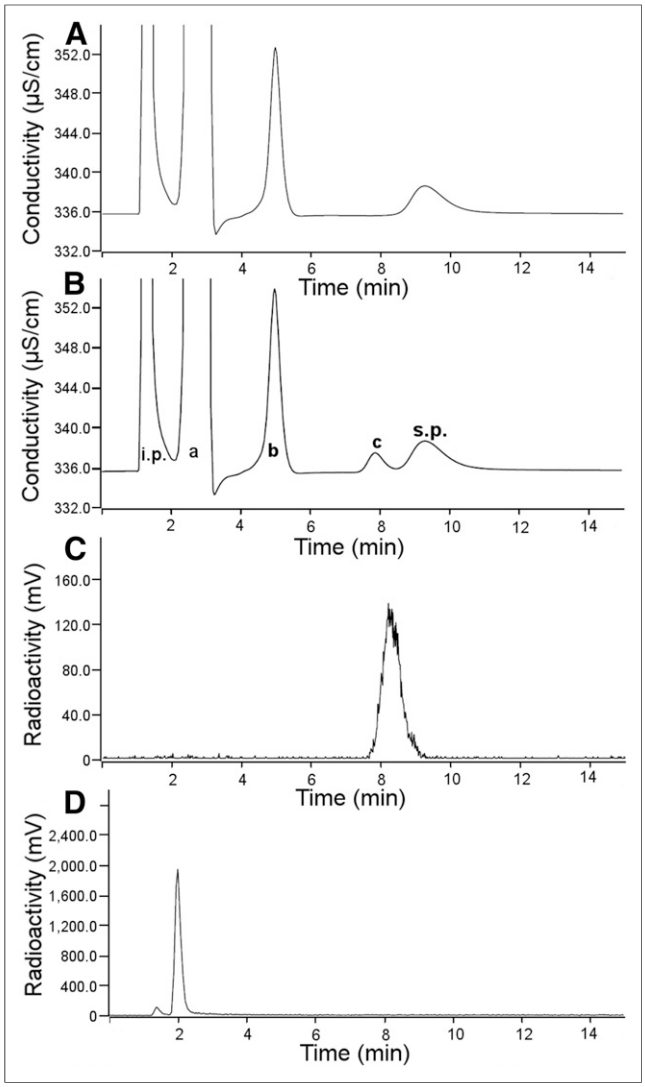

FIGURE 3. Chromatograms resulting from ion chromatography analysis of $^{18}F\text{-}SO_3F^-$: conductivity trace for no-carrier-added $^{18}F\text{-}SO_3F^-$ (A); conductivity trace for coinjection of $^{18}F\text{-}SO_3F^-$ with $^{19}F\text{-}SO_3F^-$ (80 µg/mL) (B); radioactivity trace for no-carrier-added $^{18}F\text{-}SO_3F^-$ (C); radioactivity trace for $^{18}F^-$ in H_2O (D). a = Cl^-; b = SO_4^{2-}; c = SO_3F^-; i.p. = injection peak; s.p. = system peak.

(59 ± 10 %ID/g), and salivary glands (18 ± 4 %ID/g); uptake in these organs was reduced to 4.3 ± 4.6, 3.0 ± 1.7, and 2.6 ± 1.7 %ID/g, respectively, in mice administered $NaClO_4$ (Fig. 6, and shown as SUV in Supplemental Fig. 9). The radioactivity observed in the bladder (15 ± 14 %ID/g) indicates renal excretion. A small amount of uptake in bone (17 ± 3 %ID/g) occurred and was not blocked by perchlorate, suggesting that some defluorination occurs over 2 h that was not seen during incubation in serum.

DISCUSSION

Evaluation of the inhibitory potency of fluorosulfate on hNIS confirmed its previously suggested (*9*) status as a potent inhibitor/competitive substrate with greater potency than I^- and possibly BF_4^-. The range of IC_{50} values found for both BF_4^- (currently undergoing evaluation as a clinical PET tracer for hNIS) and SO_3F^- is lower than that found for iodide (Fig. 1; Supplemental Table 1). Although inhibitory potency may not be directly indicative of ability to reach a high intracellular–extracellular concentration gradient in hNIS-expressing cells (which is the key requirement of a good PET tracer for hNIS), the data do suggest that $^{18}F\text{-}SO_3F^-$ would be a high-affinity NIS tracer. Analysis of the ionic volume (*13*) in relation to the IC_{50} of several anions against radioiodide (*10*), $^{99m}TcO_4^-$, or $^{18}F\text{-}BF_4^-$ uptake suggests that larger anions are more effective inhibitors of hNIS (Fig. 1). Accordingly, PF_6^- was found to be the most potent inhibitor examined (IC_{50}, 21 nM). However, in contrast to other known fluorine-containing NIS inhibitors, such as PF_6^- and BF_4^-, SO_3F^- has the advantage of bearing a single fluorine atom. Thus, no-carrier-added radiolabeling of SO_3F^- would yield a specific activity limited only by the ^{18}F source. We therefore chose $^{18}F\text{-}SO_3F^-$ as a target for development of a new ^{18}F-labeled hNIS tracer.

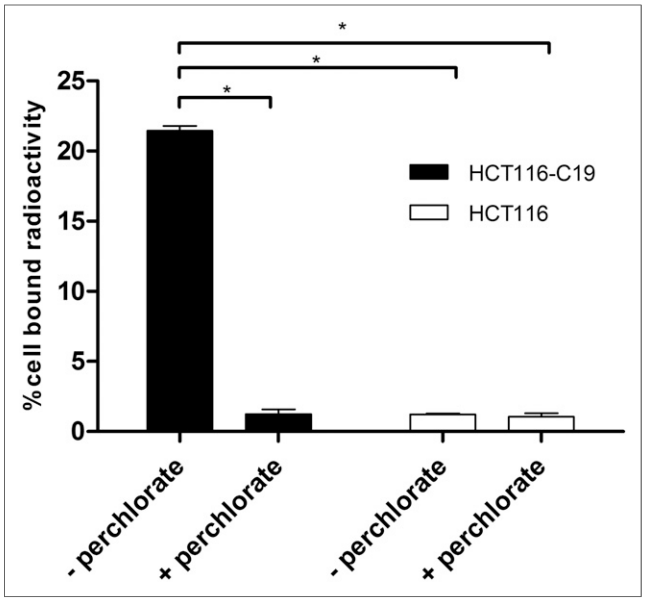

FIGURE 4. Uptake of $^{18}F\text{-}SO_3F^-$ in HCT116-C19 (hNIS-expressing) and HCT116 (hNIS-negative) cell lines in presence and absence of $NaClO_4$ (20 µM). Error bars represent SD. Intergroup differences were measured by unpaired *t* testing. $^*P < 0.00001$.

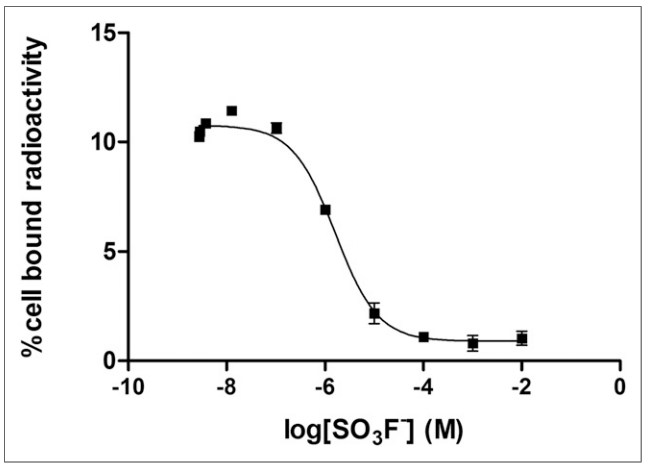

FIGURE 5. Inhibition of uptake of $^{18}F\text{-}SO_3F^-$ by $^{19}F\text{-}SO_3F^-$ in HCT116-C19 cells. Error bars represent SD. IC_{50} = 1.6 µM.

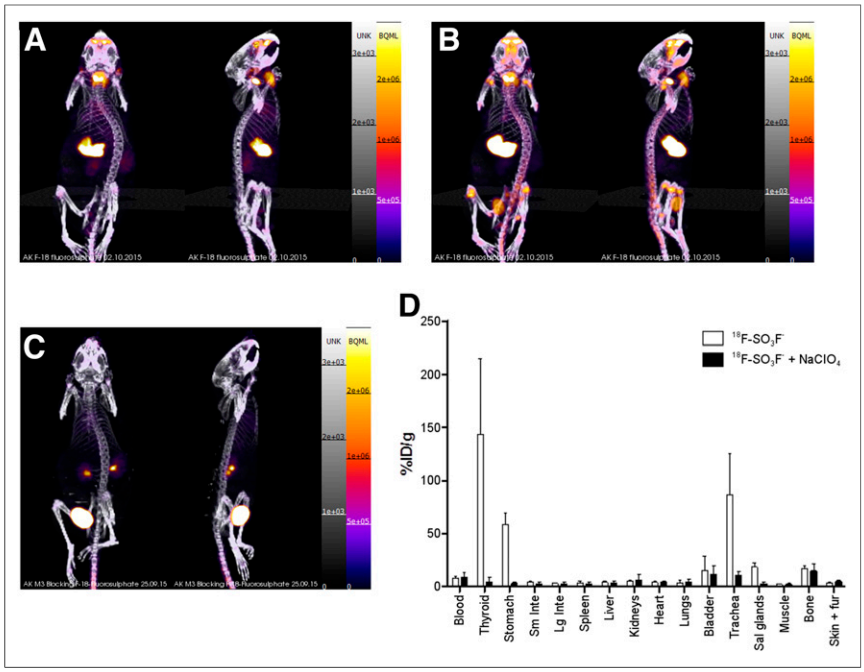

FIGURE 6. (A–C) PET/CT maximum-intensity projections of BALB/c mice 25–30 min after injection of ^{18}F-SO$_3$F$^-$ without perchlorate (A), 90–120 min after injection of ^{18}F-SO$_3$F$^-$ without perchlorate (B), and 25–30 min after injection of ^{18}F-SO$_3$F$^-$ in presence of NaClO$_4$ (250 mg/kg) (C). (D) Ex vivo biodistribution data at 2.25 h after injection (n = 3). Error bars represent SD.

Our strategy for synthesizing ^{18}F-SO$_3$F$^-$ involved using a Lewis acid–base SO$_3$–pyridine adduct, which is readily available in pure form. Radiolabeling proceeded via displacement of the pyridine by ^{18}F$^-$ followed by quenching with water to hydrolyze residual starting material to sulfate. Formation of ^{18}F-SO$_3$F$^-$, confirmed by thin-layer chromatography and ion chromatography, was observed under all reaction conditions. More basic conditions with elevated temperature and precursor concentration enhanced incorporation of ^{18}F$^-$ into ^{18}F-SO$_3$F$^-$. Further optimization may lead to improved yields, for example, using pyridine alternatives as the Lewis base in the precursor complex.

Purification using sequential alumina and quaternary methyl ammonium cartridges yielded ^{18}F-SO$_3$F$^-$ in saline, conveniently suitable for biologic use, with high radiochemical and chemical purity. The residual pyridine and K[2.2.2] in the final product were within the acceptance limits set out in the British Pharmacopoeia. The sulfate concentration resulting from precursor hydrolysis is also safe considering that MgSO$_4$ can be administered in gram quantities intravenously with minimal side effects (*21*). The specific activity of ^{18}F-SO$_3$F$^-$ (≥48.5 GBq/μmol) is significantly higher than that reported for ^{18}F-BF$_4^-$ (1 (*4*), 5 (*7*), or up to 8.8 (*22*) GBq/μmol), as there is no ^{19}F naturally present in the precursor. The specific activity is therefore limited only by that of the initial ^{18}F$^-$ and the purity of the other reagents. The method is amenable to automation, and modification of the radiosynthesis to conform to good manufacturing practices should be straightforward. The high specific activity minimizes the pharmacologic dose administered.

Assessing the biologic activity of ^{18}F-SO$_3$F$^-$ in vitro in an hNIS-expressing cell line confirmed specific NIS-mediated uptake that was absent both in hNIS-negative cells and in the presence of competitive inhibition by perchlorate. Uptake and efflux showed kinetics (equilibrium reached in under 80 min) appropriate for in vivo use. The specific activity of the ^{18}F-SO$_3$F$^-$ is very high and more than sufficient to realize the potential benefit of the high affinity: assuming an injected activity of about 10 MBq for a PET/CT scan in a mouse with an extracellular fluid volume of 5 mL, the in vivo concentration of $^{18/19}$F-SO$_3$F$^-$ will be less than 41 nM, well below the concentration at which in vitro inhibition is observed (Fig. 5). In addition to the high affinity of ^{18}F-SO$_3$F$^-$ for hNIS demonstrated by the IC$_{50}$ of 0.56 μM, the plateau intracellular-to-extracellular radioactivity concentration ratio in vitro (76:1) was higher than for either ^{99m}Tc-pertechetate (44:1) or ^{18}F-BF$_4^-$ (24:1), suggesting that—other pharmacokinetic features being similar—a higher target-to-background ratio might be expected in PET images.

PET/CT imaging of ^{18}F-SO$_3$F$^-$ in normal mice during the first hour after injection revealed uptake at sites known to express NIS. This signal was abolished by coadministration of NaClO$_4$, showing that the tracer is an excellent substrate for mouse NIS as well as hNIS. Maxima were reached in both thyroid uptake (Supplemental Fig. 5) and thyroid-to-muscle (as a background reference) uptake ratio (Supplemental Fig. 10) after 30 min, confirming this as the ideal imaging time point. Although barely detectable at 30 min (%ID/g < 1% of that in thyroid), there was increasing signal in the bones at later time points, both in PET images (Supplemental Figs. 11–13) and in the ex vivo biodistribution data. Although the in vivo hydrolysis of fluorosulfate to sulfate and fluoride is known (*23*), it is unlikely to hamper the utility of the tracer in hNIS imaging because uptake at sites of NIS expression maximizes long before bone uptake is significant.

CONCLUSION

Several fluorine-containing anions are potent hNIS inhibitors. Among them, SO$_3$F$^-$ is an hNIS inhibitor containing a single fluorine atom and has an inhibitory potency similar to or greater than that of tetrafluoroborate and greater than that of iodide. It is readily synthesized in ^{18}F-radiolabeled form in high yield, high radiochemical purity, and high specific activity. ^{18}F-SO$_3$F$^-$ shows NIS-specific uptake in vitro and in vivo and is an excellent candidate for further preclinical and clinical evaluations as an hNIS PET imaging agent for application in thyroid-related disease and hNIS reporter gene imaging. To our knowledge, this work is the first example of imaging in vivo by PET/CT using a tracer with an S–^{18}F bond. The simplicity of ^{18}F-SO$_3$F$^-$ synthesis, and its adequate in vivo stability, suggest that further attention should be given to "inorganic" ^{18}F-radiopharmaceutical synthesis (*24*) whereby atoms other than carbon, such as aluminum, silicon, boron, and now sulfur (*25*), serve as binding sites for ^{18}F.

DISCLOSURE

This work was supported by an EPSRC Industrial CASE studentship; the Biomedical Research Centre Award to Guy's & St Thomas'

NHS Foundation Trust in partnership with King's College London and King's College Hospital NHS Foundation Trust; an MRC Confidence in Concept Award administered by King's Health Partners; the Centre of Excellence in Medical Engineering funded by the Wellcome Trust and EPSRC under grant WT088641/Z/09/Z; and the King's College London and UCL Comprehensive Cancer Imaging Centre funded by the CRUK and EPSRC in association with the MRC and DoH (England). The views expressed are those of the authors and not necessarily those of the NHS, the NIHR, or the DoH. PET scanning equipment was funded by an equipment grant from the Wellcome Trust. Drs. Khoshnevisan and Blower have filed a patent relating to $^{18}F\text{-}SO_3F^-$. No other potential conflict of interest relevant to this article was reported.

REFERENCES

1. Ahn B-C. Sodium iodide symporter for nuclear molecular imaging and gene therapy: from bedside to bench and back. *Theranostics.* 2012;2:392–402.
2. Riese CGU, Seitz S, Schipper ML, Behr TM. Effective treatment of pancreatic neuroendocrine tumours transfected with the sodium iodide symporter gene by ^{186}Re-perrhenate in mice. *Eur J Nucl Med Mol Imaging.* 2009;36:1767–1773.
3. Dadachova E, Bouzahzah B, Zuckier LS, Pestell RG. Rhenium-188 as an alternative to iodine-131 for treatment of breast tumors expressing the sodium/iodide symporter (NIS). *Nucl Med Biol.* 2002;29:13–18.
4. Jauregui-Osoro M, Sunassee K, Weeks AJ, et al. Synthesis and biological evaluation of [^{18}F]tetrafluoroborate: a PET imaging agent for thyroid disease and reporter gene imaging of the sodium/iodide symporter. *Eur J Nucl Med Mol Imaging.* 2010;37:2108–2116.
5. Weeks AJ, Jauregui-Osoro M, Cleij M, Blower JE, Ballinger JR, Blower PJ. Evaluation of [^{18}F]-tetrafluoroborate as a potential PET imaging agent for the human sodium/iodide symporter in a new colon carcinoma cell line, HCT116, expressing hNIS. *Nucl Med Commun.* 2011;32:98–105.
6. Marti-Climent JM, Collantes M, Jauregui-Osoro M, et al. Radiation dosimetry and biodistribution in non-human primates of the sodium/iodide PET ligand [^{18}F]-tetrafluoroborate. *EJNMMI Res.* 2015;5:70.
7. Tonacchera M, Pinchera A, Dimida A, et al. Relative potencies and additivity of perchlorate, thiocyanate, nitrate, and iodide on the inhibition of radioactive iodide uptake by the human sodium iodide symporter. *Thyroid.* 2004;14:1012–1019.
8. Khoshnevisan A, Jauregui-Osoro M, Shaw K, et al. [^{18}F]tetrafluoroborate as a PET tracer for the sodium/iodide symporter: the importance of specific activity. *EJNMMI Res.* 2016;6:34.
9. Anbar M, Guttmann S, Lewitus Z. Effect of monofluorosulphonate, difluorophosphate and fluoroborate ions on the iodine uptake of the thyroid gland. *Nature.* 1959;183:1517–1518.
10. Waltz F, Pillette L, Ambroise Y. A nonradioactive iodide uptake assay for sodium iodide symporter function. *Anal Biochem.* 2010;396:91–95.
11. Lange W, Booth HS, Kendall F. Ammonium difluophosphate. In: Fernelius WC, ed. *Inorganic Syntheses.* Hoboken, NJ: John Wiley & Sons, Inc.; 1946:157–158.
12. Fruhwirth GO, Diocou S, Blower PJ, Ng T, Mullen GED. A whole-body dual-modality radionuclide optical strategy for preclinical imaging of metastasis and heterogeneous treatment response in different microenvironments. *J Nucl Med.* 2014;55:686–694.
13. Jenkins HDB, Roobottom HK, Passmore J, Glasser L. Relationships among ionic lattice energies, molecular (formula unit) volumes, and thermochemical radii. *Inorg Chem.* 1999;38:3609–3620.
14. Trotter J, Whitlow SH. The structures of cæsium and rubidium difluorophosphates. *J Chem Soc A.* 1967:1383–1386.
15. McDonald BJ, Tyson GJ. The crystal structures of caesium, ammonium and potassium pertechnetates. *Acta Crystallogr.* 1962;15:87.
16. Krebs B, Hasse KD. Refinements of the crystal structures of $KTcO_4$, $KReO_4$ and OsO_4: the bond lengths in tetrahedral oxoanions and oxides of d^0 transition metals. *Acta Crystallogr B.* 1976;32:1334–1337.
17. Kuntzsch M, Lamparter D, Brüggener N, Müller M, Kienzle GJ, Reischl G. Development and successful validation of simple and fast TLC spot tests for determination of Kryptofix® 2.2.2 and tetrabutylammonium in ^{18}F-labeled radiopharmaceuticals. *Pharmaceuticals (Basel).* 2014;7:621–633.
18. Tahara M, Inoue T, Miyakura Y, et al. Cell diameter measurements obtained with a handheld cell counter could be used as a surrogate marker of G2/M arrest and apoptosis in colon cancer cell lines exposed to SN-38. *Biochem Biophys Res Commun.* 2013;434:753–759.
19. Rugh R. The mouse thyroid and radioactive iodine (I-131). *J Morphol.* 1951;89: 323–365.
20. Lecat-Guillet N, Ambroise Y. Discovery of aryltrifluoroborates as potent sodium/iodide symporter (NIS) inhibitors. *ChemMedChem.* 2008;3:1207–1209.
21. Demirkaya Ş, Vural O, Dora B, Topçuoğlu MA. Efficacy of intravenous magnesium sulfate in the treatment of acute migraine attacks. *Headache.* 2001;41:171–177.
22. Huailei J, Bansal A, Pandey M, et al. Synthesis of ^{18}F-tetrafluoroboratevia radiofluorination of boron trifluoride and evaluation in a murine C6-glioma tumor model. *J Nucl Med.* 2016;57:1454–1459.
23. Mendrala AL, Markham DA, Eisenbrandt DL. Rapid uptake, metabolism, and elimination of inhaled sulfuryl fluoride fumigant by rats. *Toxicol Sci.* 2005;86: 239–247.
24. Smith GE, Sladen HL, Biagini SCG, Blower PJ. Inorganic approaches for radiolabelling biomolecules with fluorine-18 for imaging with positron emission tomography. *Dalton Trans.* 2011;40:6196–6205.
25. Inkster JAH, Liu K, Ait-Mohand S, et al. Sulfonyl fluoride-based prosthetic compounds as potential ^{18}F labelling agents. *Chemistry.* 2012;18:11079–11087.